

Article

Properties of Manganese(III) Ferrocenyl- β -Diketonato Complexes Revealed by Charge Transfer and Multiplet Splitting in the Mn 2p and Fe 2p X-Ray Photoelectron Envelopes

Blenerhassitt E. Buitendach ¹, Elizabeth Erasmus ¹, J. W. (Hans) Niemantsverdriet ² and Jannie C. Swarts ^{1,*}

¹ Department of Chemistry, University of the Free State, Bloemfontein 9300, South Africa; blenerbuitendach@gmail.com (B.E.B.); ErasmusE@ufs.ac.za (E.E.)

² SynCat@DIFFER, Syngaschem BV, De Zaale 20, Eindhoven 5612 AJ, The Netherlands; j.w.niemantsverdriet@tue.nl

* Correspondence: swartsjc@ufs.ac.za; Tel.: +27-51-401-2781

Academic Editor: Jeremy M. Rawson

Received: 9 September 2016; Accepted: 19 October 2016; Published: 26 October 2016

Abstract: A series of ferrocenyl-functionalized β -diketonato manganese(III) complexes, $[\text{Mn}(\text{FcCOCHCOR})_3]$ with $\text{R} = \text{CF}_3, \text{CH}_3, \text{Ph}$ (phenyl) and Fc (ferrocenyl) was subjected to a systematic XPS study of the Mn 2p_{3/2} and Fe 2p_{3/2} core-level photoelectron lines and their satellite structures. A charge-transfer process from the β -diketonato ligand to the Mn(III) metal center is responsible for the prominent shake-up satellite peaks of the Mn 2p photoelectron lines and the shake-down satellite peaks of the Fe 2p photoelectron lines. Multiplet splitting simulations of the photoelectron lines of the Mn(III) center of $[\text{Mn}(\text{FcCOCHCOR})_3]$ resemble the calculated Mn 2p_{3/2} envelope of Mn³⁺ ions well, indicating the Mn(III) centers are in the high spin state. XPS spectra of complexes with unsymmetrical β -diketonato ligands (i.e., R not Fc) were described with two sets of multiplet splitting peaks representing *fac* and the more stable *mer* isomers respectively. Stronger electron-donating ligands stabilize *fac* more than *mer* isomers. The sum of group electronegativities, $\Sigma\chi_{\text{R}}$, of the β -diketonato pendant side groups influences the binding energies of the multiplet splitting and charge transfer peaks in both Mn and Fe 2p_{3/2} photoelectron lines, the ratio of satellite to main peak intensities, and the degree of covalence of the Mn–O bond.

Keywords: manganese; ferrocene; β -diketonato complexes; multiplet splitting; charge transfer; X-ray photoelectron spectroscopy

1. Introduction

Properties of metal(III) β -diketonato complexes $[\text{M}(\text{R}^1\text{COCHCOR}^2)_3]$, $\text{M} = \text{metal}$ and $\text{R} = \text{pendant } \beta\text{-diketonato side groups such as } \text{CH}_3$, have been studied with a variety of different techniques including crystallography [1], electrochemistry [2], non-linear refractive measurements [3], UV-Vis spectroscopy [4], and high frequency electron paramagnetic resonance (EPR) [5]. However, characterization of these complexes by means of X-ray photoelectron spectroscopy (XPS) is not well established. XPS can play an important role in further determining the influence of the chemical environment surrounding the elements under investigation. The binding energy of a photoelectron line generally gives insight into the oxidation state of the metal ion. However, the position and shape of the photoelectron line is further influenced by final-state effects of the metal ions. These final state effects include multiplet splitting, shake-up, and shake-down peaks which are caused by crystal field splitting and charge transfer from the ligand to the metal (back bonding) [6,7]. The substructure

obtained due to Mn 2p ($2p^53d^{n+1}$) final state effect can be traced back to the 3d core-level and the valence band of the manganese. For octahedral structures such as Mn(β -diketonato)₃ complexes, the crystal field splits the 3d level into a higher energy doubly degenerate (e_g) level and a lower energy triply degenerate (t_{2g}) level. The crystal potential determines the difference between the e_g level and t_{2g} level, and this difference is large for octahedral complexes. If the interaction between the unpaired core p-electrons (2p core holes) and the unpaired valence 3d-electrons are strong enough, satellite shake-up peaks which result from valence electrons being transferred to unoccupied states are present in the XPS spectra at a few eV higher than the main photoelectron lines.

Multiplet splitting of photoelectron lines arises from the coupling of the angular momenta (spin-orbit coupling) of the unpaired core p-electrons (caused by photoionization) and the unpaired valence d-electrons [8,9]. Paramagnetic high-spin metal species show significant multiplet splitting [10]. The full width at half maximum (FWHM) of the photoelectron lines of these high-spin metals are broader than those of their low-spin counterparts—e.g., high spin Mn(III) vs. low spin Mn(II) [5]. These complex photoelectron lines can be deconvoluted with multiplet splitting peaks as demonstrated by Gupta and Sen [8,9] and others [11–13].

In the XPS of complexes bearing 3d transition metals there normally appear shake-up peaks at a few eV higher than the main peak's binding energy. This is generally accepted to be the charge transfer peak from the ligand orbital to the metal 3d, 4s, or 4p orbitals [14–19].

Multiplet splitting in XPS spectra of metal oxides and metal hydroxides has been investigated intensively [10,13,20–22]. There also are reports on multiplet splitting of metal halides, phosphates, and metal sulphides [13,22]. It has, however, never been attempted to deconvolute the multiplet splitting of Mn β -diketonates and relate the peaks to the free ion splitting as calculated by Gupta and Sen [8,9].

Useful mathematical relationships exist between the Gordy group electronegativity [23], χ_R , of different pendent R-groups of the β -diketonato ligands, ($R^1COCHCOR^2$)[−] and other physical properties including NMR resonance positions, redox potentials, reaction rates, and ligand pK_a's [24–31]. With respect to XPS determined binding energies we recently reported [4] that for [Mn(FcCOCHCOR)₃] complexes with R = CF₃, 1, CH₃, 2, C₆H₅, 3, and Fc, 4, as well as [Mn(CH₃COCHCOCH₃)₃], 5, and [Mn(FcCOCHCOFc)₂(FcCOCHCOCH₃)], 6, (Figure 1) linear relationships exist between the binding energies at maximum peak height of the Fe 2p_{3/2} and Mn 2p_{3/2} photoelectron lines and R-group's Gordy scale group electronegativities, χ_R , as well as $\Sigma\chi_R = \chi_{R1} + \chi_{R2}$ where R¹ and R² are the group electronegativities of pendant side groups of the β -diketonato ligands ($R^1COCHCOR^2$)[−] [4]. However, χ_R , and $\Sigma\chi_R$ may also relate to the substructures (shake-up, shake-down, and multiplet splitting) of the Mn 2p_{3/2} and Fe 2p_{3/2} photoelectron lines [32].

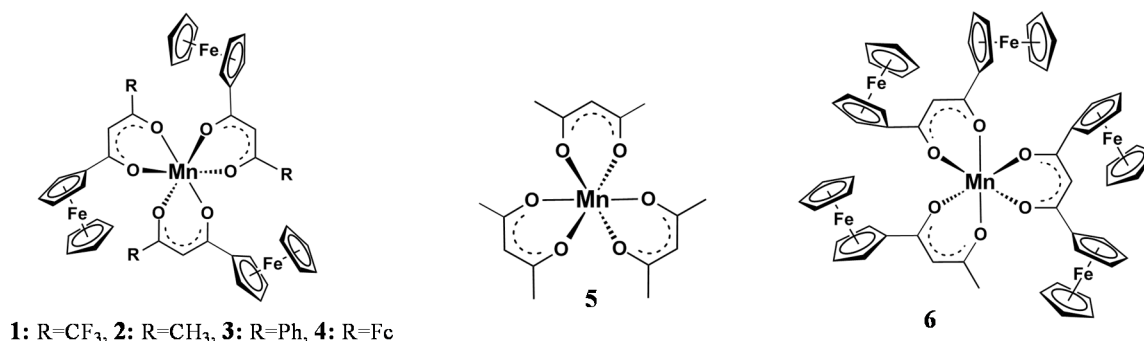


Figure 1. Structures of 1–6.

Here, we report results from an in depth analysis of the (a) satellite substructure as well as (b) multiplet splitting substructure of the manganese(III) and ferrocenyl iron(II) metal centers

and empirically quantify these substructure binding energies as a function of χ_R and $\Sigma\chi_R$ of the ligand R-groups.

2. Results and Discussion

XPS data of the β -diketonato manganese(III) complexes 1–6 (Figure 1) with respect to the Mn 2p and Fe 2p regions are presented in Tables 1–3. The broad peaks of the Mn 2p_{3/2} and Mn 2p_{1/2} photoelectron lines (a wide envelope) are located between 641.31–641.86 eV and 652.82–653.56 eV respectively (Figure 2, Table 1).

Table 1. χ_R and $\Sigma\chi_R$ values, maximum binding energies, BE, of the main Mn 2p_{3/2} envelope, full width at half maximum (FWHM) values, peak separations between main Mn 2p_{3/2} and 2p_{1/2} peaks (ΔBE_1), peak separations between satellite and Mn 2p_{3/2} peaks (ΔBE_2), I_{ratio} values, *mer* and *fac* isomer maximum binding energies of the main Mn 2p_{3/2} simulated peaks of 1–6.

| Comp. No.; Ligand R-Groups | χ_R | $\Sigma\chi_R$ ⁴ | BE Mn 2p _{3/2} (eV) | FWHM (eV) | ΔBE_1 ⁵ (eV) | ΔBE_2 ⁶ (eV) | I_{ratio} ⁷ | BE Mn 2p _{3/2} (eV) | |
|--|----------|-----------------------------|---------------------------------|--------------|------------------------------------|------------------------------------|--------------------------|------------------------------|----------------|
| | | | | | | | | <i>mer</i> | <i>fac</i> |
| 1; CF ₃ ¹ | 3.01 | 14.64 | 641.86 | 4.64 | 11.96 | 3.98 | 0.13 | 641.62 | 642.22 |
| 2; CH ₃ ¹ | 2.34 | 12.63 | 641.53 | 4.00 | 11.79 | 4.42 | 0.19 | 641.5 | 641.9 |
| 3; C ₆ H ₅ ¹ | 2.21 | 12.24 | 641.50 | 3.86 | 11.76 | 4.51 | 0.18 | 641.38 | 641.68 |
| 4; Fc ¹ | 1.87 | 11.22 | 641.31 | 3.86 | 11.58 | 4.74 | 0.23 | - ⁸ | - ⁶ |
| 5; CH ₃ ,CH ₃ ² | 2.34 | 14.04 | 641.73 | 4.06 | 11.91 | 4.36 | 0.17 | - ⁸ | - ⁸ |
| 6; Fc,Fc,CH ₃ ³ | - | 11.69 | 641.41 | 4.3 | 11.67 | 4.64 | 0.23 | - ⁹ | - ⁹ |

¹ For [Mn(FcCOCHCOR)₃], 1–4; ² For [Mn(CH₃COCHCOCH₃)₃], 5; ³ For [Mn(FcCOCHCOFc)₂(FcCOCHCOCH₃)], 6; ⁴ Sum of R-group electronegativities, $\Sigma\chi_R$. By way of example, for 6, this is calculated as follows: $\Sigma\chi_R = 5(\chi_{Fc}) + \chi_{CH_3} = 5(1.87) + 2.34 = 11.69$; ⁵ $\Delta BE_1 = BE_{Mn2p_{1/2}} - BE_{Mn2p_{3/2}}$; ⁶ $\Delta BE_2 = BE_{Mn2p_{3/2}^{satel}} - BE_{Mn2p_{3/2}^{main}}$; ⁷ $I_{ratio} = \text{ratio between the intensities of the satellite and main Mn 2p}_{3/2} \text{ photoelectron lines} = (I_{Mn2p_{3/2}^{satel}})/(I_{Mn2p_{3/2}^{main}})$; ⁸ Symmetrical ligands implying there are no *mer* and *fac* isomers; ⁹ The ligands of complex 6 are not equivalent, hence the concepts *mer* and *fac* isomers are not applicable.

The binding energy position of the binding energies at maximum peak height of the main Mn 2p_{3/2} photoelectron line corresponds to Mn^{III} [33]. It is known that Mn^{III} exists in a high-spin paramagnetic state [34,35], which also is evident from the high FWHM (ca. 3.86–4.64 eV). A strong satellite peak at ca. 4.4 eV higher than the maximum binding energy of the Mn 2p photoelectron lines is also present (Figure 2). An additional unidentified peak at ca. 8 eV higher than the maximum binding energy of the Mn 2p_{3/2} photoelectron line (prominently observed for 2, 3, 4, and 6, and to a lesser extent for 1 and 5) was observed.

A spin orbit splitting of 11.58–11.96 eV was observed, depending on $\Sigma\chi_R$ of the R-group on the β -diketonato ligand. An increase in $\Sigma\chi_R$ leads to an increase in binding energy (Figure 3a, we discussed this relationship in detail before) and the spin orbit splitting between the Mn 2p_{3/2} and Mn 2p_{1/2} photoelectron lines (Figure 3b). The latter relationship is an indication of dependence on the degree of delocalization of the spin density on the valence orbitals [36,37].

In paramagnetic compounds, the intensity of the satellite and main peaks are important. The ratio of the intensities of the satellite and main Mn 2p_{3/2} photoelectron lines, $I_{ratio} = (I_{Mn2p_{3/2}^{satel}})/(I_{Mn2p_{3/2}^{main}})$, correlates with spin density (magnetic moment, i.e., increasing number of unpaired electrons) [38,39]. Here we demonstrate that I_{ratio} (and therefore also spin density) also correlates to $\Sigma\chi_R$, Figure 3c. To interpret this relationship, we note the amount of unpaired electrons in all Mn(III) complexes 1–6 are the same. This implies the effect of the increase in polarity (electron density shift to one side of the β -diketonato ligand) of the valence electrons due to increased $\Sigma\chi_R$ could be considered proportional to the increased magnetic moment or spin density. Therefore, there must be a correlation between the spin density and the electronegativity of the ligand. From Figure 3c (and values for I_{ratio} in Table 1) it is evident that the lower $\Sigma\chi_R$ is ($\Sigma\chi_{Fc} = 11.22$ for 4 is the smallest), the larger the satellite peak gets.

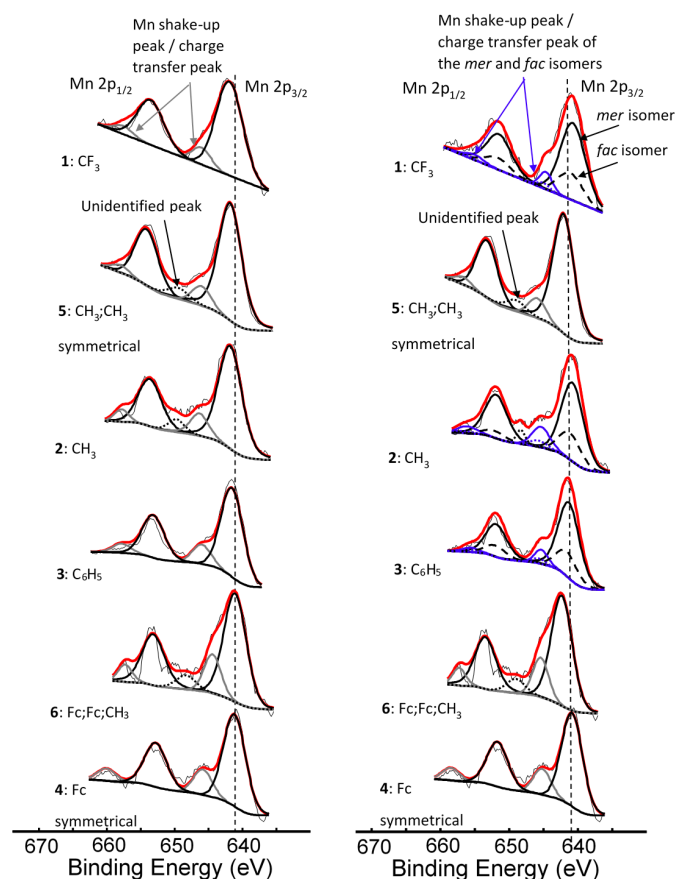


Figure 2. **Left:** Comparative XPS spectra showing a single peak fitted for all the main Mn 2p peaks as well as the shake-up peaks of the Mn 2p area of complexes 1–4, [Mn(FcCOCHCOR)₃], 5, [Mn(CH₃COCHCOCH₃)₃] and 6, [Mn(FcCOCHCOF)₂(FcCOCHCOCH₃)]. **Right:** Comparative XPS spectra showing one peak fitted for the main Mn 2p peaks of the complexes having symmetrical β -diketonato ligands and two simulated peaks for the complexes with unsymmetrical β -diketonato ligands, representing the *mer* and *fac* isomers (a ratio of 3:1 was forced into the simulation) as well as the shake-up peaks of the Mn 2p area of complexes 1–6. In some cases, a surface peak from the interface of Mn complexes attached to the carbon tape was identified and is shown with \cdots lines. The vertical dotted lines give an indication of how the binding energy shifts.

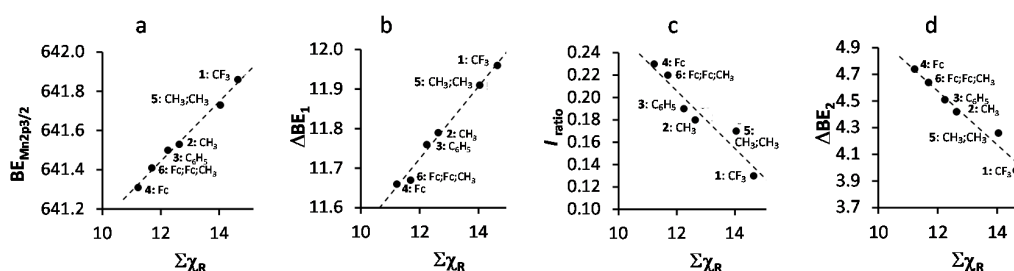


Figure 3. (a) Relationship between the binding energy of the main Mn 2p_{3/2} photoelectron envelope and the sum of β -diketonato ligand Gordy scale R-group electronegativities, $\Sigma\chi_R$, of 1–6; (b) Relationship between the spin orbit splitting of the main Mn 2p_{3/2} and Mn 2p_{1/2} photoelectron envelopes ($\Delta BE_1 = BE_{Mn2p1/2} - BE_{Mn2p3/2}$) and $\Sigma\chi_R$; (c) Relationship between the ratio of the intensities of the satellite and main Mn 2p_{3/2} photoelectron line, $I_{ratio} = (I_{Mn2p3/2satel}) / (I_{Mn2p3/2main})$, and $\Sigma\chi_R$ of 1–6; (d) Relationship between the difference between the maximum binding energy of the main Mn 2p_{3/2} photoelectron line and the satellite Mn 2p_{3/2} photoelectron line ($\Delta BE_2 = BE_{Mn2p3/2satel} - BE_{Mn2p3/2main}$) and $\Sigma\chi_R$ of 1–6.

It is known that observed satellite peaks for first row transition metal complexes with an octahedral symmetry is attributed to charge transfer from ligand-to-metal transitions of the type $e_g-e_g^*$ and/or $t_{2g}-t_{2g}^*$ [40]. A donor-acceptor bond is formed, which transfers electron density from the ligand to the metal center via a σ -donor mechanism. A larger satellite charge transfer peak indicates that more charge (electron density) is transferred from the ligand to the metal. The graph in Figure 3c confirms this. Since β -diketonato ligands with lower $\Sigma\chi_R$ values, e.g., $\Sigma\chi_{Fc} = 11.22$ for **4** which supports in total 6 strongly electron-donating ferrocenyl groups in its structure, are stronger electron-donating than others, they would transfer more charge to the Mn metal center than the ligands of, for example, **1** with three Fc and three CF_3 groups and $\Sigma\chi_R = 14.64$. Thus, our obtained relationship between $\Sigma\chi_R$ and I_{ratio} is consistent with the argument that more electron-donating ligands would transfer more charge to the metal center they are coordinated to than weaker electron-donating ligands.

The molecular orbital energy of a Mn-ligand bond depends on the overlap of the Mn 4s orbitals and ligand orbitals. Larger overlap of metal and ligand orbitals will lead to a lower energy of the bonding orbital and a higher energy of the anti-bonding orbital. Since the ligand orbitals have a lower energy than the 4s orbital of the metal center, the bonding orbital will predominantly be located over the ligand orbital, while the antibonding orbital will then mainly be located over the metal center 4s orbital. The satellite XPS peak represents the charge-transfer process from the ligand 3d orbital to the metal 4s orbital. Therefore, the difference between the maximum binding energy of the satellite Mn $2p_{3/2}$ photoelectron line and the main Mn $2p_{3/2}$ photoelectron line, $\Delta BE_2 = BE_{Mn2p3/2satel} - BE_{Mn2p3/2main}$ (values are summarized in Table 1), can be used as a measure of the degree of covalence of the ligand-metal bond. From Figure 3d, an increase $\Sigma\chi_R$ of the complexes **1–6** leads to a decrease in ΔBE_2 . This implies that the degree of the difference in covalency between the initial and final states of the ligand-metal bond decreases as $\Sigma\chi_R$ increases. It follows that the Mn–O bond of **1** with R = CF_3 has a considerably lower degree of difference in covalency between the initial and final states than **4** with R = Fc. This is in agreement with what was found [41] for a series of Mn-halides, where MnF_2 has a lower covalency than $MnBr_2$ (Br has a lower Pauling electronegativity [42], $\chi_{Br} = 2.96$, than F; $\chi_F = 4.00$).

The linear relationship obtained between spin orbit splitting of the Mn $2p_{3/2}$ and Mn $2p_{1/2}$ photoelectron lines (ΔBE_1), the ratio of the intensities of the satellite and main Mn $2p_{3/2}$ photoelectron line (I_{ratio}), and the difference between the maximum binding energy of the satellite Mn $2p_{3/2}$ photoelectron line and the main Mn $2p_{3/2}$ photoelectron line (ΔBE_2) on the one hand and the sum of β -diketonato ligand Gordy scale R-group electronegativities, $\Sigma\chi_R$ (Figure 3) on the other fit the equations:

$$BE_{Mn2p3/2} = 0.1517 \Sigma\chi_R + 639.62; R^2 = 0.9919 \quad (1)$$

$$\Delta BE_1 = BE_{Mn2p1/2} - BE_{Mn2p3/2} = 0.0911 \Sigma\chi_R + 10.631; R^2 = 0.9867 \quad (2)$$

$$I_{ratio} = (I_{Mn2p3/2satel}) / (I_{Mn2p3/2main}) = -0.0258 \Sigma\chi_R + 0.5148; R^2 = 0.9111 \quad (3)$$

$$\Delta BE_2 = BE_{Mn2p3/2satel} - BE_{Mn2p3/2main} = -0.2013 \Sigma\chi_R + 6.99; R^2 = 0.9621 \quad (4)$$

The above relationships enable one to calculate (or predict) the degree of delocalization of electrons, amount of charge transferred via a σ -donor mechanism, as well as the degree of the difference in covalency between the initial and final states for manganese(III) β -diketonato complexes **1–6** as well as related complexes provided the group electronegativity of β -diketonato R-group substituents are known.

The oxygen atoms of the ferrocenyl-functionalized β -diketonato manganese(III) complexes, **1–4** and **6**, as well as the *tris*(acetylacetonato)manganese(III) complexes **5** are octahedrally arranged around the Mn metal center. When the Mn(III) complexes contain symmetrically substituted β -diketonato ligands, as in **4** and **5**, the six Mn–O bonds are equal and these complexes display a D_3 symmetry. However, when the Mn(III) complexes contain unsymmetrically substituted β -diketonato ligands, as in **1–3**, *mer* and *fac* geometrical isomers are possible (Figure 4). The meridional isomers (*mer*)

possess a symmetry plane passing through the Mn metal center which is formed by the three identical substituents (in this case the ferrocenyl groups) on the three unsymmetrical ligands. For the facial isomer (*fac*), the vertices of one face of the octahedron of the Mn complexes are occupied by the same substituent (in this case the ferrocenyl groups) from the three unsymmetrical ligands.

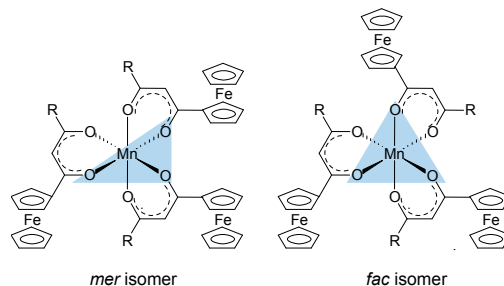


Figure 4. *Mer* and *fac* isomers of $[\text{Mn}(\text{FcCOCHCOR})_3]$ complexes containing an unsymmetrically substituted β -diketonato ligand, R = CF_3 (1), CH_3 (2), C_6H_5 (3).

For the three complexes 1–3 having unsymmetrically substituted β -diketonato ligands, two Gaussian peaks were simulated to the Mn main $2p_{3/2}$ peak as well as to the shake-up peak; one was associated with the *mer* and the other with the *fac* isomer. Since the distribution between *mer* and *fac* isomers statistically should be 3:1 for all three complexes, the two Gaussian peaks were enforced in a ratio of 3:1. This simulation with two Gaussian peaks (FWHM = 3.90, 3.68, 3.68 eV for 1, 2, and 3 respectively and CHI squared = ca. 1.3) was more accurate than the fitting of only one Gaussian peak (FWHM = 4.64, 4.00, 3.86 eV for 1, 2, and 3 respectively CHI squared = ca. 1.5) and the FWHM decreased. The peak of the *fac* isomer (dashed lines) is found at ca. 0.4 eV higher binding energy than the peak of the *mer* isomer (solid lines), see Figure 2 and Table 1. The higher binding energy of the *fac* isomer is in agreement with published results [29], as well as experimental evidence of a similar Al compound, which showed that in solution only the *mer* isomer is present [43]. This implies that the *mer* isomer is more stable and in XPS the more stable isomer would be detected at the lowest binding energy. The difference in binding energies between *mer* and *fac* isomers has, to our knowledge, not been explained theoretically before. Our XPS measurements, however, shows experimentally they are different. To place this experimental result in perspective, it is useful to note that DFT calculations on a similar set of tris(β -diketonato)manganese(III) complexes revealed there is an energy difference between *mer* and *fac* HOMO energies [44]. Since E_{HOMO} has been proven to be related to binding energies obtained from XPS [30,45,46], it follows that there must also be a difference between the binding energies of the *fac* and *mer* isomers. Qualitatively, this means interaction between different molecular fragments (Fc and R; R and Fc cannot equal in *mer* and *fac* isomers) in different special arrangements relative to each other must induce small but noticeable differences in the binding energies for these *fac* and *mer* isomers.

The difference in binding energy position for the *mer* and *fac* isomer was found to be dependent on $\Sigma\chi_{\text{R}}$, the sum of the Gordy group electronegativity of the R-groups substituted on the ferrocenyl-containing β -diketonato ligands. From Table 1, it is evident that as $\Sigma\chi_{\text{R}}$ increases, the difference between the *mer* and the *fac* isomer binding energies also increases. This implies that more electron-donating R-groups like the ferrocenyl moiety (Fc) stabilizes the *fac* isomer more than electron-withdrawing R-groups like CF_3 . The higher stability of the *fac* isomer of more electron-donating R-groups was also found with DFT calculations of similar Cr(III) and Fe(III) β -diketonato complexes [40].

The Mn(III) atom in complexes 1–6 all have an initial state $2p^63s^23p^63d^4$ subshell population. After photoionization, a final state of $2p^53s^23p^63d^4$ subshell population is present [47]. Thus the Mn 2p XPS spectra of complexes 1–6 should display a similar multiplet splitting substructure as Gupta and Sen calculated for the core p -level of the free Mn^{3+} ion [8,9]. To demonstrate that the experimentally measured Mn $2p_{3/2}$ photoelectron lines could successfully be generated by the theoretically calculated

multiplet splitting peaks of Gupta and Sen, spectra of complexes 1–6 were simulated with one set of multiplet split peaks consisting of five components according to the most intense Gupta and Sen calculated peaks for a high-spin Mn^{3+} ion (peaks 1–5, Figure 5, left) in a ratio area % the same as the calculated ratio area distributions of Gupta and Sen for the free Mn^{3+} ion. These were ca. 1:1:1.35:0.7:0.3 [8,9]. Similar successful fittings utilizing the Gupta and Sen distribution were published for manganese oxides, phosphates and sulphates [47,48].

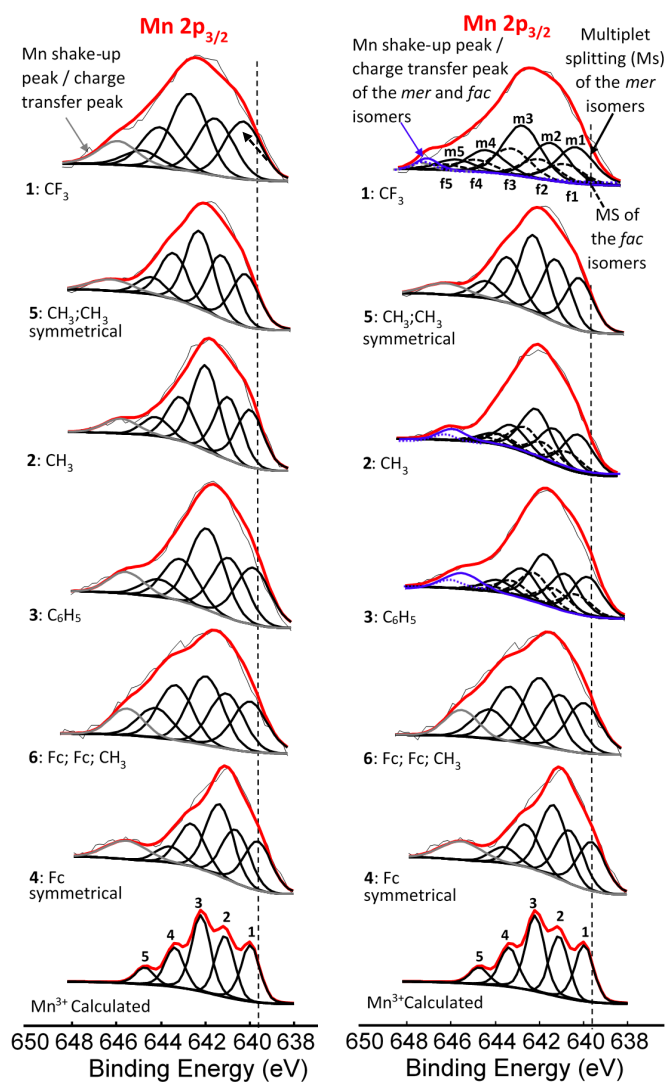


Figure 5. Left: Comparative XPS spectra showing multiplet splitting for the main $Mn\ 2p_{3/2}$ peaks as well as the shake-up peak of the $Mn\ 2p_{3/2}$ of complexes 1–6. **Right:** Multiplet splitting (Ms) of both the *mer* (solid line) *fac* (dashed line) isomers. In both XPS comparisons, simulated spectra of the Gupta and Sen calculated multiplet splitting of Mn^{3+} is superimposed onto experimental spectra. The vertical dotted lines give an indication of how binding energy shifts.

For the three complexes containing symmetrically substituted β -diketonato ligands and two separate types of ligands, complexes 4–6, the single set of five multiplet splitting peaks gave excellent fits, with a CHI squared = ca. 1.2. However, for the complexes containing unsymmetrically substituted β -diketonato ligands, 1–3, where both a *mer* isomer and *fac* isomer are possible, the fitting of two different sets of multiplet splitting peaks (labelled $m1$ – $m5$ and $f1$ – $f5$) into the broad $Mn\ 2p_{3/2}$ peak (main envelope), proved to be more accurate than the fitting of only one set of multiplet splitting peaks, to give a CHI squared = ca. 0.9 for two peaks as compared to a CHI squared = ca. 1.3 (see Figure 5 right, top).

This is an indication that two different species are present within the sample of complex 1–3. These two different species are attributed to the *mer* and *fac* isomers of the unsymmetrical substituted ferrocenyl-containing β -diketonato manganese(III) complexes. The weight % of the *mer* and *fac* isomers fitted for the XPS data was, as for Figure 2, again 3:1, due to the statistical possibility of occurrence. The XPS data of the multiplet splitting fits of the main envelope of the Mn $2p_{3/2}$ peaks are listed in Table 2. The multiplet splitting simulations correlated very well with the reported measured data of different manganese oxides, phosphates, and sulphates [47,48].

This implies that, according to the multiplet splitting simulations, the final-state obtained after photoionization of the Mn(III) species is within experimental error independent of the ligand type, even if the ligand varies from an oxide to a phosphates, sulphates, and finally to β -diketonato ligands. The measured fits of the multiplet splitting of the Mn $2p_{3/2}$ envelopes represent the calculated fittings as predicted by Gupta and Sen well; only the binding energy position differs slightly. This is to be expected since the group electronegativities of the ligands play an important role in the position of the binding energy.

The relationship between $\Sigma\chi_R$ and the binding energy of the first peak of the fitted multiplet splitting peaks of the Mn $2p_{3/2}$ photoelectron line of 4–6 and the first peak of the *mer* isomers' fitted multiplet splitting peaks of the Mn $2p_{3/2}$ photoelectron line of 1–3 (see Table 2 and Figure 6) was found to be directly proportional. With an increase in $\Sigma\chi_R$, increased electron density moves away from the Mn^{3+} metal center towards the ligand. The Mn^{3+} ion binds more firmly to its own electrons, causing the increased binding energy values.

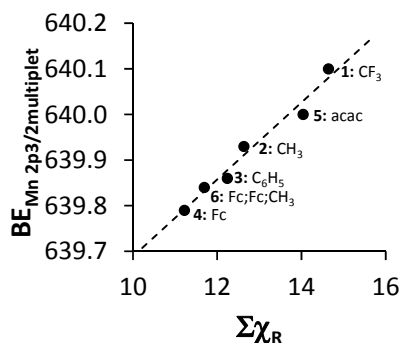


Figure 6. Relationship between the binding energy of the first peak of the *mer* isomers' fitted multiplet splitting peaks of the Mn $2p_{3/2}$ photoelectron line of 1–3 or the first peak of the fitted multiplet splitting peaks of the Mn $2p_{3/2}$ photoelectron line of 4–6 ($BE_{Mn2p_{3/2}multiplet}$) and $\Sigma\chi_R$.

The linear relationship obtained between binding energy of the first peak of the fitted multiplet splitting peaks of the Mn $2p_{3/2}$ photoelectron line of 4–6 and the first peak of the *mer* isomer fitted multiplet splitting peaks of the Mn $2p_{3/2}$ photoelectron line of 1–3 ($BE_{Mn2p_{3/2}multiplet}$) and $\Sigma\chi_R$ (Figure 6) fits the equation

$$BE_{Mn2p_{3/2}multiplet} = 0.0943 \Sigma\chi_R + 638.85; R^2 = 0.9691 \quad (5)$$

Since we could observe the charge transfer process from the β -diketonato ligand to Mn in the Mn 2p spectra, it would only be logical that we should be able to identify a similar charge transfer peak in photoelectron lines representing the ligand. The complexes under investigation are ferrocenyl-containing β -diketonates; therefore the Fe 2p photoelectron line is representative of the ligand. For complexes 1–4 and 6, the Fe $2p_{3/2}$ photoelectron lines have a maximum binding energy at ca. 708 eV, with a distinct shoulder on the lower energy side of the main photoelectron line, Figure 7. This shoulder is formed by a shake-down mechanism and it represents the charge transfer from the β -diketonato ligand to Mn. The main Fe $2p_{3/2}$ photoelectron lines are sharp single peaks and since the iron in the ferrocenyl moiety is Fe^{2+} , it is in a low spin state and does not display multiplet splitting.

Table 2. Maximum binding energy, BE, of the Mn 2p_{3/2} envelope, the binding energies of each multiplet split peak and I_{ratio} %'s for the multiplet splitting of the Mn 2p_{3/2} peak. BE of the shake-up (charge transfer peak) is also shown.

| Comp. No.; R-Groups | Max BE (eV) | Isomer | Peak ¹ (eV) | I_{ratio} % ⁷ | Peak ² (eV) | I_{ratio} % ⁷ | Peak ³ (eV) | I_{ratio} % ⁷ | Peak ⁴ (eV) | I_{ratio} % ⁷ | Peak ⁵ (eV) | I_{ratio} % ⁷ | Shake-up (eV) | I_{ratio} % ⁷ |
|--|----------------|----------------|---------------------------|----------------------------|---------------------------|----------------------------|---------------------------|----------------------------|---------------------------|----------------------------|---------------------------|----------------------------|------------------|----------------------------|
| 1; CF ₃ ¹ | 641.86 | <i>mer</i> | 640.10 | 23.4 | 641.22 | 23.4 | 642.52 | 31.2 | 644.17 | 15.0 | 645.56 | 7.0 | 646.90 | 2.46 |
| | | <i>fac</i> | 640.70 | 23.4 | 641.82 | 23.4 | 643.12 | 31.2 | 644.77 | 15.0 | 646.16 | 7.0 | | |
| 2; CH ₃ ¹ | 641.53 | <i>mer</i> | 639.93 | 23.1 | 640.99 | 23.1 | 641.83 | 31.4 | 642.93 | 15.3 | 643.71 | 7.1 | 645.77 | 4.56 |
| | | <i>fac</i> | 640.33 | 23.1 | 641.39 | 23.1 | 642.23 | 31.4 | 643.33 | 15.3 | 644.11 | 7.1 | | |
| 3; C ₆ H ₅ ¹ | 641.50 | <i>mer</i> | 639.86 | 23.0 | 640.90 | 23.0 | 641.82 | 31.0 | 642.90 | 16.0 | 644.03 | 7.0 | 645.71 | 9.28 |
| | | <i>fac</i> | 640.16 | 23.0 | 641.20 | 23.0 | 642.12 | 31.0 | 643.20 | 16.0 | 644.33 | 7.0 | | |
| 4; Fc ¹ | 641.31 | - ⁵ | 639.78 | 22.5 | 640.80 | 22.5 | 641.56 | 30.3 | 642.86 | 18.0 | 643.87 | 6.7 | 645.89 | 10.25 |
| 5; CH ₃ ,CH ₃ ² | 641.73 | - ⁵ | 640.00 | 22.9 | 641.14 | 22.9 | 642.20 | 31.0 | 643.36 | 16.1 | 644.36 | 7.1 | 646.24 | 3.98 |
| 6; Fc,Fc,CH ₃ ³ | 641.41 | - ⁶ | 639.84 | 21.5 | 640.89 | 21.5 | 641.82 | 26 | 643.19 | 21.5 | 644.10 | 11.2 | 645.35 | 8.69 |
| Mn ³⁺ ⁴ | | - | 640.1 | 23 | 641.4 | 23 | 642.3 | 31 | 643.1 | 16 | 644.9 | 7 | | |

¹ For [Mn(FcCOCHCOR)₃], 1–4. ² For [Mn(CH₃COCHCOCH₃)₃], 5. ³ For [Mn(FcCOCHCOFc)₂(FcCOCHCOCH₃)], 6. ⁴ Gupta and Sen calculations of the Mn(III) free ion [8,9].

⁵ Symmetrical ligands implying there are no *mer* and *fac* isomers. ⁶ The ligands of complex 6 are not equivalent, hence the concepts *mer* and *fac* isomers are not applicable.

⁷ I_{ratio} percentages = percentage ratio between the intensities of the satellite and main Mn 2p_{3/2} photoelectron lines (= $(I_{Mn2p3/2satel}) / (I_{Mn2p3/2main}) \times 100$).

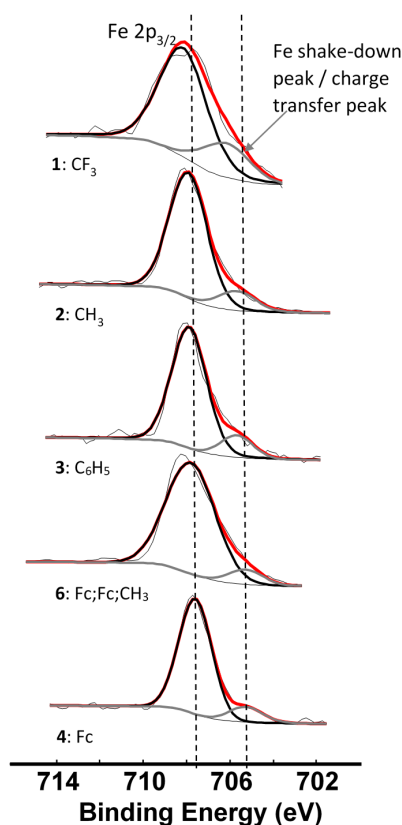


Figure 7. Comparative XPS spectra showing the main Fe $2p_{3/2}$ peaks as well as the shake-down peaks of complexes 1–4 and 6. The vertical dotted lines give an indication of how binding energy shifts.

An in-depth discussion of the main Fe 2p photoelectron lines of 1–4 and 6 were already presented before by us [4], so here only the shake down peak will be discussed. The data obtained from the XPS for the Fe $2p_{3/2}$ main and satellite peaks are summarized in Table 3. As $\Sigma\chi_R$ increases, the binding energy of the main Fe $2p_{3/2}$ photoelectron line also increases. A similar trend was observed for the Fe $2p_{3/2}$ satellite peaks (Figure 8, left, Table 3). However, the degree of increase in binding energy for the main and satellite Fe $2p_{3/2}$ peaks are not the same and the difference between the Fe $2p_{3/2}$ main and the Fe $2p_{3/2}$ satellite peaks ($\Delta BE = BE_{Fe2p3/2main} - BE_{Fe2p3/2satel}$) is inversely proportional to the $\Sigma\chi_R$ (Figure 8, middle). As $\Sigma\chi_R$ increases, the difference between the main and the satellite Fe $2p_{3/2}$ photoelectron lines, ΔBE , decreases.

Table 3. $\Sigma\chi_R$ values, maximum binding energy (BE) of the main and satellite Fe $2p_{3/2}$ envelope, peak separations between the satellite and main Fe $2p_{3/2}$ peaks ΔBE , as well as I_{ratio} values for 1–4 and 6.

| Comp. Num.; R-Groups | $\Sigma\chi_R$ ³ | $BE_{Fe2p3/2main}$ (eV) | FWHM (eV) | $BE_{Fe2p3/2satel}$ (eV) | FWHM (eV) | ΔBE ⁵ (eV) | I_{ratio} ^f |
|---|-----------------------------|-------------------------|-----------|--------------------------|----------------|-------------------------------|--------------------------|
| 1; R = CF ₃ ¹ | 14.64 | 708.03 | 2.67 | 705.91 | - ⁴ | 2.12 | 0.28 |
| 2; R = CH ₃ ¹ | 12.63 | 707.87 | 2.22 | 705.61 | 2.37 | 2.26 | 0.16 |
| 3; R = C ₆ H ₅ ¹ | 12.24 | 707.84 | 1.93 | 705.48 | 2.07 | 2.36 | 0.16 |
| 4; R = Fc ¹ | 11.22 | 707.77 | 2.81 | 705.28 | 2.40 | 2.34 | 0.09 |
| 6; Fc,Fc,CH ₃ ² | 11.69 | 707.79 | 1.95 | 705.45 | 1.95 | 2.49 | 0.11 |

¹ For [Mn(FcCOCHCOR)₃], 1–4. ² For [Mn(FcCOCHCOFc)₂(FcCOCHCOCH₃)], 6. ³ Sum of R-group electronegativities; calculations are explained in Table 1. ⁴ Due to a non-linear baseline, FWHM of 1 could not be measured with any degree of accuracy, but it is estimated as 2.84 eV. ⁵ $\Delta BE = BE_{Fe2p3/2main} - BE_{Fe2p3/2satel}$. ^f $I_{ratio} = \text{ratio between the intensities of the satellite and main Fe } 2p_{3/2} \text{ photoelectron lines } (= (I_{Fe2p3/2satel}) / (I_{Fe2p3/2main}))$.

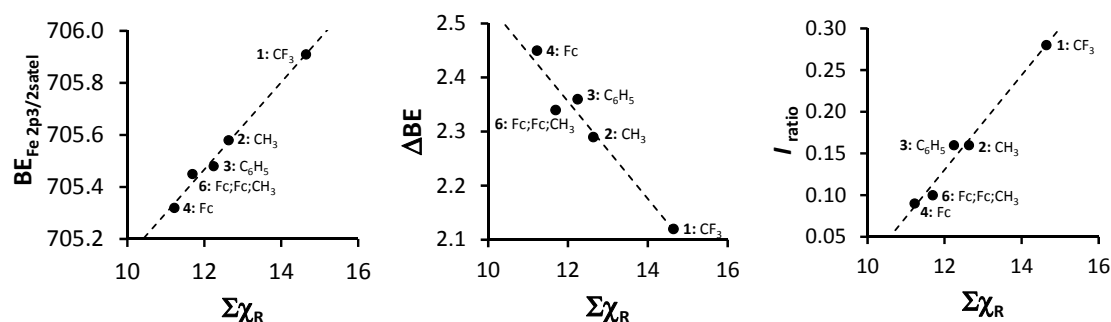


Figure 8. Left: Relationship of binding energy of the satellite Fe 2p_{3/2} photoelectron line of 1–4 and 6 ($BE_{Fe2p3/2satel}$) and the sum of β -diketonato ligand Gordy scale R-group electronegativities, $\Sigma\chi_R$. Middle: Relationship between $\Delta BE = BE_{Fe2p3/2main} - BE_{Fe2p3/2satel}$ and $\Sigma\chi_R$. Right: Relationship between $I_{ratio} = (I_{Fe2p3/2satel}) / (I_{Fe2p3/2main})$ and $\Sigma\chi_R$.

The charge transfer process takes place between the 3d orbitals of the β -diketonato ligand oxygens and the 4s of the manganese. Thus, when charge is transferred to the manganese, an electron deficiency in the β -diketonato ligand is the result. More specifically, the electron deficiency manifests at the delocalized electrons in the six-membered chelating ring of the coordinated β -diketonato ligand. Stronger electron-donating pendent β -diketonato R-groups (e.g., ferrocenyl) would be able to stabilize this electron deficiency much better than electron-withdrawing R-groups such as CF₃. This enhanced stabilization would cause the binding energy of the Fe shake-down satellite peak to be located at lower binding energies in comparison to the main Fe 2p_{3/2} photoelectron line, which explains the inverse proportional correlation.

Comparison of the ratio of intensities of the satellite and main Fe 2p_{3/2} photoelectron line ($I_{ratio} = (I_{Fe2p3/2satel}) / (I_{Fe2p3/2main})$) with $\Sigma\chi_R$ revealed a direct proportional correlation (Figure 8, right) showing that as $\Sigma\chi_R$ increases, the intensity of the satellite Fe 2p_{3/2} photoelectron line also increases. This is opposite to the trend found for the intensity ratios of the satellite and main Mn 2p_{3/2} photoelectron line vs. $\Sigma\chi_R$ (Figure 3c).

After charge transfer from the ligand to the manganese, a partially positive charge, δ^+ , is created on the six-membered chelating ring of the coordinated β -diketonato ligand. When an electron-withdrawing R-group like CF₃ is attached to this chelating ring (as in complex 1), it withdraws even more electron density causing an even bigger partial positive charge, δ^{n+} ($1 < n < 2$). To compensate for this overly δ^{n+} charge, the electron-donating ferrocenyl groups on the other side of each of the β -diketonato ligands, donates extra electron density to the chelating pseudo-aromatic β -diketonato ring. This causes the intensity of the Fe 2p_{3/2} shake-down peak to be relatively large. When there are two electron-donating ferrocenyl groups on each coordinating β -diketonato ligand, as in 4, more ferrocenyl groups donate electron-density to compensate for the δ^{n+} charge. Thus, the individual contributions from each ferrocenyl group (and also the intensity of the charge transfer peak) will be less than for complex 1 bearing CF₃ electron-withdrawing groups.

The linear relationship obtained between binding energy of the satellite Fe 2p_{3/2} photoelectron line of 1–4 and 6 ($BE_{Fe2p3/2satel}$), the difference between the maximum binding energy of the main and satellite Fe 2p_{3/2} photoelectron lines ($\Delta BE = BE_{Fe2p3/2main} - BE_{Fe2p3/2satel}$) as well as the intensity ratios of the satellite and main Fe 2p_{3/2} photoelectron lines ($I_{ratio} = (I_{Fe2p3/2satel}) / (I_{Fe2p3/2main})$) and the sum of β -diketonato ligand Gordy scale R-group electronegativities, $\Sigma\chi_R$ (Figure 8) fit the equations:

$$BE_{Fe2p3/2satel} = 0.1678 \Sigma\chi_R + 703.45; R^2 = 0.9885 \quad (6)$$

$$\Delta BE = -0.0899 \Sigma\chi_R + 3.4344; R^2 = 0.9456 \quad (7)$$

$$I_{ratio} = 0.0568 \Sigma\chi_R - 0.5505; R^2 = 0.9794 \quad (8)$$

3. Methods

3.1. Compounds

The ferrocenyl-functionalized β -diketonato manganese(III) complexes of general formula $[\text{Mn}(\text{FcCOCHCOR})_3]$, with $\text{R} = \text{CF}_3$, **1**, CH_3 , **2**, C_6H_5 , **3** and Fc , **4**, as well as $[\text{Mn}(\text{CH}_3\text{COCHCOCH}_3)_3]$, **5**, and $[\text{Mn}(\text{FcCOCHCOFc})_2(\text{FcCOCHCOCH}_3)]$, **6**, (Figure 1) were prepared and characterized according to published methods [4].

3.2. X-Ray Photoelectron Spectroscopy

XPS data was recorded on a PHI 5000 Versaprobe (Ulvac-Phi, Chigasaki, Japan) system, with a monochromatic Al $K\alpha$ X-ray source. Spectra were obtained using the aluminium anode (Al $K\alpha = 1486.6$ eV), operating at 50 μm , 12.5 W, and 15 kV energy (97 X-ray beam). A low energy neutralizer electron gun was used to minimize charging of the samples. The instrument work function was calibrated to give a binding energy of 284.5 eV for the lowest binding energy peak of the carbon 1s envelope, corresponding to adventitious carbon. Survey scans were recorded at constant pass energy of 187.85 eV, while detailed region scans were recorded at constant pass energy of 29.35 eV for C and O, and 93.90 eV for Fe and Mn. The resolution of the PHI 5000 Versaprobe system is FWHM = 0.53 eV at a pass energy of 23.5 and FWHM = 1.44 eV at a pass energy of 93.90. The background pressure was 2×10^{-8} mbar. Spectra have been charge-corrected to the main line of the carbon 1s spectrum, which was set to 284.5 eV. XPS data was analyzed utilizing Multipak version 8.2c computer software [49] and applying Gaussian/Lorentz fits (the Gaussian/Lorentz ratios were always > 95%). All measured photoelectron lines were seven-point smoothed.

4. Concluding Remarks

The sub-structures of the Mn 2p and Fe 2p XPS photoelectron lines gave insight into the electronic structure of the $[\text{Mn}(\beta\text{-diketonato})_3]$ complexes **1–6**. Despite the absence of fine structure, the Mn $2p_{3/2}$ envelope could successfully be described with the calculated multiplet splitting from Gupta and Sen [8,9]. The Mn $2p_{3/2}$ envelopes of complexes containing unsymmetrically substituted β -diketonato ligands could be approximated by two sets of calculated multiplet splitting peaks corresponding to the presence of *mer* and *fac* isomers. The shake-up peak in the Mn 2p and the shake-down peak in the Fe 2p region gave a clear indication of the charge transfer process taking place from the ligand to the centrally coordinated Mn^{III} cation. A key factor that influences all these processes and binding energies is the theoretical concept “sum of group electronegativities”, $\Sigma\chi_{\text{R}}$, of the β -diketonato pendant side groups. Utilizing the experimental XPS binding energies and $\Sigma\chi_{\text{R}}$ values, it was shown that the *mer* isomer is more stable than the *fac* isomer but more electron-donating ligands stabilize *fac* isomers more than *mer* isomers. It also became possible to explain the intuitive feeling that ligands which are stronger electron-withdrawing induces a lower degree of covalence in bonds than ligands which are stronger electron-donating and that the latter transfer more charge to metal centers to which they are coordinated than electron-withdrawing ligands. Furthermore, it also explains the decrease in binding energy of core electrons of metals when relative stronger electron-donating ligands are coordinated to it. Variations in the XPS spectral characteristics of the Mn and Fe 2p regions as a result of changing R-group substituted on the β -diketonato ligands, $(\text{FcCOCHCOR})^-$, as well as their influence on the electronic environment of the central coordinated high spin Mn^{III} cation, is emphasized by the linear relationships involving on the one hand $\Sigma\chi_{\text{R}}$ and on the other, binding energies of the satellite and main Fe and Mn $2p_{3/2}$ photoelectron lines of **1–4** and **6**, the difference between the maximum binding energy of the main and satellite Fe and Mn $2p_{3/2}$ photoelectron lines or the intensity ratios between satellite and main Fe or Mn $2p_{3/2}$ photoelectron lines.

Acknowledgments: J.C.S., E.E., and B.E.B. acknowledge financial support from the NRF under grant 2054243, the UFS and Syngaschem BV during the course of this study. Syngaschem BV acknowledges substantial funding from Synfuels China Technology Co., Ltd., (Huairou, Beijing, China).

Author Contributions: B.E.B. synthesized all compounds; E.E. recorded all XPS spectra; J.W.N., E.E., and J.C.S. interpreted all XPS data, all authors assisted in writing the manuscript.

Conflicts of Interest: The authors declare no conflict of interest.

References and Notes

1. Banske, W.; Ludwig, E.; Mickler, W.; Uhlemann, E.; Hahn, E.; Lügger, T.; Lehmann, A. Mangan(IV)-Komplexe mit Dreizähnigen Diaciden Liganden. Kristallstruktur von Acetylacetonato-salicylaldehydbenzoylhydrazonato (2-)-methanol-mangan(III). *Z. Anorg. Allg. Chem.* **1995**, *621*, 1483–1488. [[CrossRef](#)]
2. Perera, I.R.; Gupta, A.; Xiang, W.; Daeneke, T.; Bach, U.; Evans, R.A.; Ohlin, C.A.; Spiccia, L. Introducing manganese complexes as redox mediators for dye-sensitized solar cells. *Phys. Chem. Chem. Phys.* **2014**, *16*, 12021–12028. [[CrossRef](#)] [[PubMed](#)]
3. Henari, F.Z.; Ali-Mohamed, A.Y. Nonlinear refractive index measurement of tris(acetylacetonato) manganese(III) solution. *Opt. Laser Technol.* **2008**, *40*, 602. [[CrossRef](#)]
4. Buitendach, B.E.; Erasmus, E.; Landman, M.; Niemantsverdriet, J.W.; Swarts, J.C. Consequences of electron-density manipulations on the X-ray photoelectron spectroscopic properties of ferrocenyl- β -diketonato complexes of manganese(III). Structure of $[\text{Mn}(\text{FcCOCHCOCH}_3)_3]$. *Inorg. Chem.* **2016**, *55*, 1992–2000. [[CrossRef](#)] [[PubMed](#)]
5. Barra, A.L.; Gatteschi, D.; Sessoli, R.; Abbati, G.L.; Cornia, A.; Fabretti, A.C.; Uytterhoeven, M.G. Electronic structure of manganese(III) compounds from high-frequency EPR spectra. *Angew. Chem. Int. Ed.* **1997**, *36*, 2329–2331. [[CrossRef](#)]
6. Kowalczyk, S.P.; Ley, L.; Martin, R.L.; McFeely, F.R.; Shirley, D.A. Relaxation and final-state structure in XPS of atoms, molecules and metals. *Faraday Discuss. Chem. Soc.* **1975**, *60*, 7–17. [[CrossRef](#)]
7. Chusuei, C.C.; Goodman, D.W. Control of CuO Particle Size on SiO₂ by Spin Coating. In *Encyclopedia of Physical Science and Technology*, 3rd ed.; Meyers, R.A., Ed.; Academic Press: New York, NY, USA, 2001; Volume 17, p. 921.
8. Gupta, R.P.; Sen, S.K. Calculation of multiplet structure of core p -vacancy levels. *Phys. Rev. B* **1974**, *10*, 71–77. [[CrossRef](#)]
9. Gupta, R.P.; Sen, S.K. Calculation of multiplet structure of core p -vacancy levels. II. *Phys. Rev. B* **1975**, *12*, 15–19. [[CrossRef](#)]
10. Biesinger, M.C.; Payne, B.P.; Grosvenor, A.P.; Lau, A.W.M.; Gerson, A.R.; Smart, R.S.C. Resolving surface chemical states in XPS analysis of first row transition metals, oxides and hydroxides: Cr, Mn, Fe, Co and Ni. *Appl. Surf. Sci.* **2011**, *257*, 2717. [[CrossRef](#)]
11. Ünveren, E.; Kemnitz, E.; Hutton, S.; Lippitz, A.; Unger, W.E.S. Analysis of highly resolved X-ray photoelectron Cr 2p spectra obtained with a Cr₂O₃ powder sample prepared with adhesive tape. *Surf. Interface Anal.* **2004**, *36*, 92–95. [[CrossRef](#)]
12. Ilton, E.S.; de Jong, W.A.; Bagus, P.S. Intra-atomic many-body effects in p -shell photoelectron spectra of Cr³⁺ ions. *Phys. Rev. B* **2003**, *68*, 125106. [[CrossRef](#)]
13. Biesinger, M.C.; Brown, C.; Mycroft, J.R.; Davidson, R.D.; McIntyre, N.S. X-ray photoelectron spectroscopy studies of chromium compounds. *Surf. Interface Anal.* **2004**, *36*, 1550–1563. [[CrossRef](#)]
14. Asada, S.; Sugano, S. Satellites in X-ray photoelectron Spectra of Transition-Metal Compounds. *J. Phys. Soc. Jpn.* **1976**, *41*, 1291–1299. [[CrossRef](#)]
15. Larsson, S. Satellites in ESCA inner-shell spectra of 3d⁰ transition metal complexes. *J. Electron Spectrosc. Relat. Phenom.* **1976**, *8*, 171–178. [[CrossRef](#)]
16. Larsson, S. Shake-up and multiplet structure of ESCA satellites of Cu compounds. *Chem. Phys. Lett.* **1976**, *40*, 362–366. [[CrossRef](#)]
17. Larsson, S.; Braga, M. Charge transfer satellites. Intensity dependence on localization of hole state. *Chem. Phys. Lett.* **1977**, *48*, 596–600. [[CrossRef](#)]
18. Carlson, T.A. *Photoelectron and Auger Spectroscopy*; Plenum: New York, NY, USA, 1976.
19. Feuerbacher, B.; Fitton, B.; Willis, R.F. *Photoemission and the Electronic Properties of Surfaces*; Wiley: New York, NY, USA, 1978.

20. Biesinger, M.C.; Payne, B.P.; Hart, B.R.; Grosvenor, A.P.; McIntyre, N.E.; Lau, L.W.M.; Smart, R.S.C. Quantitative chemical state XPS analysis of first row transition metals, oxides and hydroxides. *J. Phys. Conf. Ser.* **2008**, *100*, 012026. [[CrossRef](#)]
21. Grosvenor, A.P.; Biesinger, M.C.; Smart, R.S.C.; McIntyre, N.S. New interpretations of XPS spectra of nickel metal and oxides. *Surf. Sci.* **2006**, *600*, 1771–1779. [[CrossRef](#)]
22. Grosvenor, A.P.; Kobe, B.A.; Biesinger, M.C.; McIntyre, N.S. Investigation of multiplet splitting of Fe 2p XPS spectra and bonding in iron compounds. *Surf. Interface Anal.* **2004**, *36*, 1564–1574. [[CrossRef](#)]
23. Gordy scale group electronegativities, χ_R , are empirical numbers that express the combined tendency of not only one atom, but a group of atoms, like R = CF₃ or ferrocenyl (Fc), to attract electrons (including those in a covalent bond) as a function of the number of valence electrons, n , and the covalent radius, r (in Å), of groups as discussed in Kagarise, R.E., Relation between the electronegativities of adjacent substituents and the stretching frequency of the carbonyl group. *J. Am. Chem. Soc.* **1955**, *77*, 1377–1379. [[CrossRef](#)].
24. Erasmus, E.; Conradie, J.; Muller, A.; Swarts, J.C. Synthesis, crystal structure and electrochemistry of tetrahedral mono- β -diketonato titanocenyl complexes. *Inorg. Chim. Acta* **2007**, *360*, 2277–2283. [[CrossRef](#)]
25. Erasmus, E. Ferrocene- and ruthenocene-containing chalcones: A spectroscopic and electrochemical study. *Inorg. Chim. Acta* **2011**, *378*, 95–101. [[CrossRef](#)]
26. Muller, T.J.; Conradie, J.; Erasmus, E. A spectroscopic, electrochemical and DFT study of *para*-substituted ferrocene-containing chalcone derivatives: Structure of FcCOCHCH(*p*-^tBuC₆H₄). *Polyhedron* **2012**, *33*, 257–266. [[CrossRef](#)]
27. Erasmus, E. Swarts, J.C. Intramolecular communication and electrochemical observation of the 17-electron ruthenocenium cation in fluorinated ruthenocene-containing β -diketones; polymorphism of C₁₀H₂₁ and C₁₀F₂₁ derivatives. *New J. Chem.* **2013**, *37*, 2862–2873. [[CrossRef](#)]
28. Conradie, M.M.; Conradie, J.; Erasmus, E. Immobilization of iron tris(β -diketonates) on a two-dimensional flat amine functionalized silicon wafer: A catalytic study of the formation of urethane, from ethanol and a diisocyanate derivative. *Polyhedron* **2014**, *79*, 52–59. [[CrossRef](#)]
29. Erasmus, E. Synthesis and unexpected electrochemical reaction of *p*-substituted phenyl diphenylphosphinites. *J. Electroanal. Chem.* **2014**, *727*, 1–7. [[CrossRef](#)]
30. Liu, R.; Conradie, J.; Erasmus, E. Comparison of X-ray photoelectron spectroscopy multiplet splitting of Cr 2p peaks from chromium tris(β -diketonates) with chemical effects. *J. Electron Spectrosc. Relat. Phenom.* **2016**, *206*, 46–51. [[CrossRef](#)]
31. Erasmus, E. Synthesis and electrochemistry of *p*-substituted phenyl diphenylphosphinite rhodium(I) complexes. *Polyhedron* **2016**, *106*, 18–26. [[CrossRef](#)]
32. Carniato, S.; Journal, L.; Guillemin, R.; Piancastelli, M.N.; Stolte, W.C. A new method to derive electronegativity from resonant inelastic X-ray scattering. *J. Chem. Phys.* **2016**, *137*, 144303–144313. [[CrossRef](#)] [[PubMed](#)]
33. Ilton, E.S.; Post, J.E.; Heaney, P.J.; Ling, F.T.; Kerisit, S.N. XPS determination of Mn oxidation states in Mn (hydr)oxides. *Appl. Surf. Sci.* **2016**, *366*, 475–485. [[CrossRef](#)]
34. Wang, S.; He, W.R.; Ferbinteanu, M.; Li, Y.H.; Huang, E. Tetragonally compressed high-spin Mn(III) Schiff base complex: Synthesis, crystal structure, magnetic properties and theoretical calculations. *Polyhedron* **2013**, *52*, 1199–1205. [[CrossRef](#)]
35. Kennedy, B.J.; Murray, K.S. Magnetic properties and zero-field splitting in high-spin manganese(III) complexes. 1. Mononuclear and polynuclear Schiff-base chelates. *Inorg. Chem.* **1985**, *24*, 1557. [[CrossRef](#)]
36. Carver, J.C.; Schweitzer, G.K.; Carlson, T.A. Use of X-ray Photoelectron Spectroscopy to Study Bonding in Cr, Mn, Fe, and Co Compounds. *J. Chem. Phys.* **1972**, *57*, 973–981. [[CrossRef](#)]
37. Ivanova, T.M.; Shchukarev, A.V.; Naumkin, A.V.; Sidorov, A.A.; Kiskin, M.A.; Novotortsev, V.M.; Eremenko, I.L. X-ray photoelectron spectra of polynuclear manganese complexes. *Russ. J. Inorg. Chem.* **2008**, *53*, 1929–1933. [[CrossRef](#)]
38. Borod'ko, Y.G.; Vetchinkin, S.I.; Zimont, S.L.; Ivleva, I.N.; Shul'ga, Y.M. Nature of satellites in X-ray photoelectron spectra XPS of paramagnetic cobalt (II) compounds. *Chem. Phys. Lett.* **1976**, *42*, 264–267. [[CrossRef](#)]
39. Ioffe, M.S.; Borod'ko, Y.G. Dependence of satellite intensity in X-ray photoelectron spectra of Cu(II) complexes on the spin density on copper. *J. Electron Spectrosc. Relat. Phenom.* **1977**, *11*, 235–238. [[CrossRef](#)]
40. Perera, J.S.H.Q.; Frost, D.C.; McDowell, C.A. X-ray photoelectron spectroscopy of Co(II), Ni(II), and Cu(II) acetylacetonate vapors. *J. Phys. Chem.* **1980**, *72*, 5151–5158. [[CrossRef](#)]

41. Park, J.; Ryu, S.; Han, M.; Oh, S.J. Charge-transfer satellites in the 2p core-level photoelectron spectra of heavy-transition-metal dihalides. *Phys. Rev. B* **1988**, *37*, 10867–10875. [[CrossRef](#)]
42. Pauling, L. The nature of the chemical bond. IV The energy of single bonds and the relative electronegativity of atoms. *J. Am. Chem. Soc.* **1932**, *54*, 3570–3582. [[CrossRef](#)]
43. Gericke, H.J.; Muller, A.J.; Swarts, J.C. Electrochemical illumination of intramolecular communication in ferrocene-containing tris- β -diketonato aluminum(III) complexes; cytotoxicity of Al(FcCOCHCOCF₃)₃. *Inorg. Chem.* **2012**, *51*, 1552–1561. [[CrossRef](#)] [[PubMed](#)]
44. Gotstynski, R.; van Rooyen, P.H.; Conradie, J. Jahn-Teller distortion in tris[4,4,4-trifluoro-1-(2-thienyl)-1,3-butanedionato]manganese(III) isomers: An X-ray and computational study. *J. Mol. Struct.* **2016**, *1119*, 48–53. [[CrossRef](#)]
45. Conradie, J.; Erasmus, E. XPS Fe 2p peaks from iron tris(β -diketonates): Electronic effect of the β -diketonato ligand. *Polyhedron* **2016**, *119*, 142–150. [[CrossRef](#)]
46. Jansen van Rensburg, A.; Landman, M.; Erasmus, E.; van der Westhuizen, D.; Ferreira, H.; Conradie, M.M.; Conradie, J. Electrochemical and X-ray photoelectron spectroscopic insights into Molybdenum(0) Fischer ethoxycarbene complexes. *Electrochim. Acta* **2016**, *219*, 204–213. [[CrossRef](#)]
47. Nelson, A.J.; Reynolds, J.G.; Roos, J.W. Core-level satellites and outer core-level multiplet splitting in Mn model compounds. *J. Vac. Sci. Technol. A* **2000**, *18*, 1072–1076. [[CrossRef](#)]
48. Nesbitt, H.W.; Banerjee, D. Interpretation of XPS Mn(2p) spectra of Mn oxyhydroxides and constraints on the mechanism of MnO₂ precipitation. *Am. Mineral.* **1998**, *83*, 305–315. [[CrossRef](#)]
49. Moulder, F.; Stickle, W.F.; Sobol, P.E.; Bomben, K.D. *Handbook of X-ray Photoelectron Spectroscopy*; ULVAC-PHI, Inc.: Chigasaki, Japan, 1995; pp. 45, 57 and 143.

Sample Availability: Not Available.



© 2016 by the authors; licensee MDPI, Basel, Switzerland. This article is an open access article distributed under the terms and conditions of the Creative Commons Attribution (CC-BY) license (<http://creativecommons.org/licenses/by/4.0/>).